J Mater Sci: Mater Electron (2016) 27:10780–10790
DOI 10.1007/s10854-016-5183-0

Hydrothermal synthesis, multicolor tunable luminescence and energy transfer of Eu^{3+} or/and Tb^{3+} activated $NaY(WO_4)_2$ nanophosphors

Yan Liu[1] · Guixia Liu[1] · Jinxian Wang[1] · Xiangting Dong[1] · Wensheng Yu[1] · Tingting Wang[1]

Received: 13 April 2016 / Accepted: 11 June 2016 / Published online: 20 June 2016
© Springer Science+Business Media New York 2016

Abstract Eu^{3+} and/or Tb^{3+} doped $NaY(WO_4)_2$ nanomaterials have been successfully synthesized by one-step hydrothermal method. The samples were characterized by X-ray diffraction, field-emission scanning electron microscopy, X-ray energy dispersive spectroscopy, and photoluminescence spectra. The results show that the novel nanoplates with a diameter of 300–600 nm and the thickness of 20–25 nm are observed. Under the excitation of 246 or 230 nm, individual RE^{3+} ions activated $NaY(WO_4)_2$ phosphors exhibit excellent emission properties in their respective regions. The as-prepared Eu^{3+} or Tb^{3+} doped samples show strong red and green emission, originating from the allowed $^5D_0 \rightarrow {}^7F_J$ ($J = 0, 1, 2$) transition of the Eu^{3+} ions and the $^5D_4 \rightarrow {}^7F_J$ ($J = 6, 5, 4, 3$) transition of the Tb^{3+} ions. In addition, by properly tuning the relative concentration of Eu^{3+} ions in the case of Eu^{3+} and Tb^{3+} co-doped systems, tunable emissions in a single component are obtained under the excitation of 230 or 395 nm. Moreover, an energy transfer from Tb^{3+} to Eu^{3+} is observed, which has been justified through the luminescence spectra and the fluorescence decay curves. Furthermore, the corresponding luminescence and energy transfer mechanism have been proposed in optical transitions and possible energy transfer scheme. These results indicate that Eu^{3+} and Tb^{3+} doped $NaY(WO_4)_2$ phosphors will find potential application in the field of solid-state lighting.

✉ Guixia Liu
liuguixia22@163.com

[1] Key Laboratory of Applied Chemistry and Nanotechnology at Universities of Jilin Province, Changchun University of Science and Technology, Changchun 130022, China

1 Introduction

Nowadays, inorganic luminescent materials containing rare-earth (RE) ions have become desirable in the development of optical materials. These materials have interesting optical characteristics and high potentiality in the fields of light-emitting diodes (LEDs), solid state lasers, display systems and other optoelectronic devices due to their luminescent properties largely based on the abundant emission colors deriving from the rare-earth ions [1–4]. Among them, white light-emitting diodes (W-LEDs) have been intensively studied as an attractive alternative to conventional lamps because of their excellent luminescent characteristics, good stability, high luminescence efficiency, as well as low cost [5, 6]. Phosphors are efficient luminescence materials and irreplaceable components for the development of LEDs. Recently, oxide phosphors for LEDs have gained interest due to their better thermal and chemical stability and environmental friendliness compared with sulfides, such as $Y_2O_2S:Eu^{3+}$, $Ca_{1-x}Sr_xS:Eu^{2+}$ and ZnCdS:Ag red phosphors, ZnS:Cu, Al, $SrGa_2S_4:Eu^{2+}$ green phosphors and ZnS:Ag blue phosphors [7–10], which are currently used for multicolor lighting or white lighting.

Obviously, the characteristic emissions of luminescent materials result from interactions between host and rare-earth ions used as luminescent centers. To design and achieve excellent luminescent performance, the proper host material is often indispensable. Tungstates are well-known classical self-activated luminescence materials, which can effectively absorb ultraviolet (UV) and X-ray, then simultaneously migrate the absorbed energy to the doped rare-earth ions through energy transfer, and give their characteristic emissions. Therefore, they are recently considered as promising host materials for rare-earth luminescent centers because of the special properties of WO_4^{2-}

group [11–14]. From the report of Huang et al. [15], it was seen that tungstate host essentially showed a little weaker blue emission at room temperature compared to the absorption in excitation spectrum, owing to efficient energy transfer from WO_4^{2-} group to activators. Liu et al. [16] had also discovered that $NaY(WO_4)_2$ exhibited a broad emission centered at approximately 469 nm without doping Ln^{3+} ions, and the intensity of this emission decreased when Ln^{3+} ions were doped.

Among them, alkali rare earth tungstates ($ARE(WO_4)_2$, where A = alkali metal ions, RE = rare earth ions) are of particular interest in the potential applications in quantum electronics, visual light display system, solid-state lighting, and optoelectronic devices [17–20]. They especially had been studied widely as luminescent host in the field of solid state lasers in the past years. Furthermore, as the most frequently used and studied rare earth ions in luminescent materials, Eu^{3+} has been investigated primarily in red phosphors. Also, Tb^{3+} ions are used often for their characteristic green emission. Generally, white light emissions or individual color emissions can be achieved by systematically altering relative rare-earth ion concentration and largely depend on the energy transfer of excitation energy between rare-earth ions. Reasonable adjusting the relative dopant contents of sensitizer and activator in the case of Eu^{3+} and Tb^{3+} co-doped systems can be an effective approach to obtain multiple colors, even in some special host materials, and nearly white light for W-LEDs excited by UV light can be obtained [17–21]. Furthermore, in Eu^{3+} and Tb^{3+} co-doped systems, there is an energy transfer from Tb^{3+} to Eu^{3+} obviously, such as the unique luminescent properties of Eu^{3+}, Tb^{3+} co-doped SrY_2O_4 [21] and Sr_3AlO_4F [22], the dipole–dipole type energy transfer between Tb^{3+} and Eu^{3+} in $NaLa(WO_4)_2$ [23], the energy transfer from Tb^{3+} to Eu^{3+} via its 5d and 4f states in $Ba_3La(PO_4)_3$ [24] and $Tb_2(WO_4)_3$:Eu^{3+} nanowires [25].

In order to search for a new and economical as well as high efficient phosphor, many researches have been focused on alkali rare earth tungstates. For example, Zheng et al. [12] obtained white phosphors by single doping Eu^{3+} in the $NaY(WO_4)_2$. Li et al. [26] prepared high brightness $MLa(WO_4)_2$:Eu^{3+} (M = Li, Na, K) and $NaRE(WO_4)_2$:Eu^{3+} (RE = Gd, Y, Lu) red phosphors. To date, tungstates doped with different rare earth ions have been prepared most maturely through high temperature solid state reaction [16, 20, 26, 27], and industrial productions of rare earth tungstates are all obtained by this method. However, there are some insurmountable defects in high temperature solid state reaction such as high temperature, long time, high energy consumption making more high-cost and depletion of energy. In consideration of this problem, the hydrothermal method is preferred because the synthesis conditions such as temperature and reaction time can be easily adjusted. Furthermore, the hydrothermal process has proved to be a facile and fast route with low cost and energy consumption, which has been widely employed for the synthesis of inorganic materials including alkali rare earth tungstates [11, 12, 28–30]. Among the alkali rare earth tungstates, the $NaY(WO_4)_2$ lattice belongs to the scheelite $CaWO_4$ structures, which consists of two formula units in the unit cell, with space group C_{4h}^6 (I41/a). Na^+ and Y^{3+} ions are equivalent, and occupy sites of symmetry S_4. Due to the entire disorder among the occupation of these atoms in their sites, for simplicity we consider them as identical. The two equivalent W^{6+} ions occupy sites of symmetry S_4, the eight oxygen atoms are equivalent, and occupy a site of symmetry C_1 [31].

In 2004, Neeraj et al. [20] prepared the $NaY(WO_4)_{2-x}(MoO_4)_x$:Eu^{3+} red phosphors by high temperature solid state method, which might find application in white lighting devices utilizing GaN-based excitation in the n-UV. Liu et al. [27] prepared $NaY(WO_4)_2$:Tb^{3+} powders by solid state reaction at 900 °C for 6 h. Also, a few more reports had been found on the synthesis of Eu^{3+} or Tb^{3+} activated $NaY(WO_4)_2$ host lattice [27–29, 32]. In our previous reports, we prepared $NaLa(WO_4)_2$:Er^{3+}, Eu^{3+} phosphors [33], Tb^{3+} or/and Sm^{3+} doped $NaGd(WO_4)_2$ phosphors [34] and Tm^{3+}, Dy^{3+}, Eu^{3+} co-doped $NaGd(WO_4)_2$ phosphors [35]. However, to the best of our knowledge, no reports have been found on the Eu^{3+} and Tb^{3+} co-doped $NaY(WO_4)_2$ phosphors and the energy transfer mechanism between them in this host.

In this work, we reported the synthesis of Eu^{3+} and Tb^{3+} doped $NaY(WO_4)_2$ phosphors by a facile hydrothermal process without further sintering treatment. Moreover, we investigated the energy transfer from WO_4^{2-} group to Eu^{3+} and Tb^{3+}, respectively. In addition, by adjusting the doping concentration of Eu^{3+} ions in the case of Eu^{3+} and Tb^{3+} co-doped systems, an energy transfer from Tb^{3+} to Eu^{3+} was observed and tunable emission colors were realized in these materials by changing the doping concentration of Eu^{3+}. Finally, the main mechanism for energy transfer between Tb^{3+} and Eu^{3+} in the $NaY(WO_4)_2$ phosphors was analyzed.

2 Experimental sections

2.1 Materials

Aqueous solutions of $Y(NO_3)_3$, $Eu(NO_3)_3$ and $Tb(NO_3)_3$ were obtained by dissolving the rare earth oxides Ln_2O_3 (Ln = Y, Eu) (99.99 %) and Tb_4O_7 (99.99 %) in dilute HNO_3 solution (15 mol/L) under heating with agitation in ambient atmosphere. All the other chemicals were of

analytic grade and used as received without further purification.

2.2 Methods

A series of rare earth-doped $NaY(WO_4)_2$ phosphors were synthesized by a facile hydrothermal process without further sintering treatment. 1.0 mmol of $RE(NO_3)_3$ [including $Y(NO_3)_3$, $Eu(NO_3)_3$ or $Tb(NO_3)_3$] were added into 10 mL of aqueous solution containing 2.0 mmol of glycine. After vigorous stirring for 20 min, 2.0 mmol of $Na_2WO_4{\cdot}2H_2O$ was slowly added dropwise into the above solution. After additional agitation for 30 min, the resultant milky colloidal suspension was transferred to a Teflon bottle held in a stainless steel autoclave, and then heated at 260 °C for 2 h. Finally, as the autoclave was naturally cooled to room-temperature, the precipitates were separated by centrifugation, washed with deionized water and ethanol in sequence each several times, and then dried in air at 60 °C for 12 h. Specific material formula is shown in Table 1.

2.3 Characterization

The purity and phase structure of the products were examined by X-ray powder diffraction (XRD) performed on a Rigaku D/max-RA X-ray diffractometer with Cu Kα radiation ($\lambda = 0.15406$ nm) and Ni filter, operating at 20 mA, 30 kV, scanning speed, step length and diffraction range were 10°/min, 0.1° and 10°–80°, respectively. The morphology and composition of the samples were observed by a FEI XL-30 field emission scanning electron microscope (FESEM) equipped with an energy-dispersive X-ray spectrometer (EDS). The excitation and emission spectra, and the luminescence decay curves of samples were recorded with a HITACHI F-7000 Fluorescence Spectrophotometer using a Xe lamp as the excitation source, scanning at 1200 nm/min.

3 Results and discussion

3.1 Crystallization behavior and structure

The XRD patterns of $NaY(WO_4)_2$:Eu^{3+}, Tb^{3+} phosphors have been shown in Fig. 1. It is obvious that all the diffraction peaks of these samples are in good agreement with pure tetragonal $NaY(WO_4)_2$ in I41/a space group (lattice constants a = b = 5.205 Å, c = 11.251 Å, JCPDS card 48-0886) and no other phases or impurities can be detected. This result indicates that the complete crystallinity and pure-phase double alkaline rare-earth tungstates with the general formula of $NaY(WO_4)_2$ can be obtained by one-step hydrothermal method and the Eu^{3+} ions and Tb^{3+} ions are completely incorporated into the $NaY(WO_4)_2$ host lattice without making significant changes to the crystal structure. Moreover, the high crystallinity is still obtained by low temperature. Typically, the doped ions occupy sites in the host largely depending on the effective radii (r) of the cations. The effective radii of the Tb^{3+} ions (0.1044 nm for CN = 8) and the Eu^{3+} ions (0.1066 nm for CN = 8) are similar to those of the Y^{3+} ions (0.1019 nm for CN = 8). In view of the effective radii, Tb^{3+} and Eu^{3+} ions are expected to occupy the Y^{3+} sites preferentially because the radii of the Na^{+} ions (0.118 nm) are too large for Tb^{3+} and Eu^{3+} ions as well as the valence state analysis.

3.2 Morphology and composition

The morphology and composition features of $NaY(WO_4)_2$:0.03Eu^{3+} phosphor were investigated by FESEM and EDS, as shown in Figs. 2a–c. The FESEM images reveal that it is composed of regular nanoplates with the diameter from 300 to 600 nm and the thickness ranging from 20 to 25 nm (Fig. 2a, b). The plate-like morphology formation may be resulted from the addition of glycine, which is acted as a surfactant to control the shape of the samples, the similar role can be seen in other Ref. [36]. EDS pattern shown in Fig. 2c performs the

Table 1 Specific material formula of $NaY(WO_4)_2$:Eu^{3+}, Tb^{3+}

Samples	$Na_2WO_4{\cdot}2H_2O$ (mmol)	$Y(NO_3)_3$ (mmol)	$Eu(NO_3)_3$ (mmol)	$Tb(NO_3)_3$ (mmol)
$NaY(WO_4)_2$:0.02Tb^{3+}	2.0	0.98	0	0.02
$NaY(WO_4)_2$:0.03Tb^{3+}	2.0	0.97	0	0.03
$NaY(WO_4)_2$:0.005Eu^{3+}, 0.02Tb^{3+}	2.0	0.975	0.005	0.02
$NaY(WO_4)_2$:0.01Eu^{3+}, 0.02Tb^{3+}	2.0	0.97	0.01	0.02
$NaY(WO_4)_2$:0.02Eu^{3+}, 0.02Tb^{3+}	2.0	0.96	0.02	0.02
$NaY(WO_4)_2$:0.03Eu^{3+}, 0.02Tb^{3+}	2.0	0.95	0.03	0.02
$NaY(WO_4)_2$:0.03Eu^{3+}	2.0	0.97	0.03	0

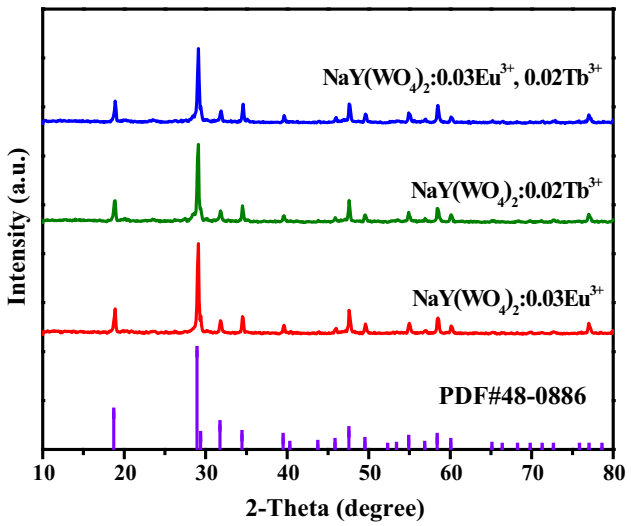

Fig. 1 X-ray powder diffraction patterns of NaY $(WO_4)_2$:Eu^{3+}, Tb^{3+} phosphors

chemical composition of the product, containing Na, Y, Eu, W, and O (silicon and gold signals are from silicon host and spraying gold process). Combined with the above XRD patterns, the samples are further proved to be $NaY(WO_4)_2$.

3.3 Photoluminescence properties

Room temperature photoluminescence spectra of the synthesized $NaY(WO_4)_2$ nanocrystals doped with Ln^{3+} were investigated. Figure 3 shows the PL and PLE spectra of $NaY(WO_4)_2$:Tb^{3+}, $NaY(WO_4)_2$:Eu^{3+}, and $NaY(WO_4)_2$:-Eu^{3+}, Tb^{3+} phosphors. It is well known that the excitation spectrum of $NaY(WO_4)_2$:0.02Tb^{3+} (monitored at 545 nm) consists of two components. The former is a strong and broad band from 200 to 300 nm with a maximum at about 230 nm due to f-d transitions of Tb^{3+} and O^{2-}–W^{6+} charge transfer transitions within the WO_4^{2-} groups, which was deconvolved into two bands using Gaussian fitting shown in Fig. 4a. The peak located at 226 nm is due to the f-d transitions of Tb^{3+} and the peak centered at 264 nm is due to the CTB of WO_4^{2-}. The latter is the weak f-f transitions of Tb^{3+} in the longer wavelength region, whose are hardly detected. They are located at 341, 352, 359, 369, 378 and 488 nm corresponding to the transitions from the $^7F_6$ ground state to the different excited states of Tb^{3+}, namely, $^5G_2$, $^5D_2$, $^5G_5$, $^5G_6$, $^5D_3$ and $^5D_4$, respectively, which are shown in Fig. 3c. The PL spectrum of the 2 mol% Tb^{3+} activated $NaY(WO_4)_2$ nanocrystals by exciting at 230 nm is shown in Fig. 3a (right). It can be seen that there are two groups of emissions. The first broad band from 410–540 nm with a maximum at about 450 nm belongs to the blue emission of WO_4^{2-} group. The second group of emission bands locates at 488 nm in the blue region and 545 nm in the green region, which belong to $^5D_4 \rightarrow {}^7F_6$ and $^5D_4 \rightarrow {}^7F_5$ transitions of Tb^{3+}, respectively. Compared Fig. 3a, b, it can be seen that for $NaY(WO_4)_2$:Tb^{3+} phosphors, with a lower doping concentration of Tb^{3+} (shown in Fig. 3a), the blue emission of WO_4^{2-} centered at 450 nm is strong. As Tb^{3+} concentration increases, the emission of WO_4^{2-} is depressed owing to the more energy transfer from WO_4^{2-} group to Tb^{3+}, which enhances the transitions of $^5D_4$ to ^7F_j of Tb^{3+} with a green emission (Fig. 3b, right). Figure 3d shows the PLE and PL spectra of $NaY(WO_4)_2$:0.03Eu^{3+} phosphor. The PLE spectrum monitored with 616 nm emission ($^5D_0$–$^7F_2$)

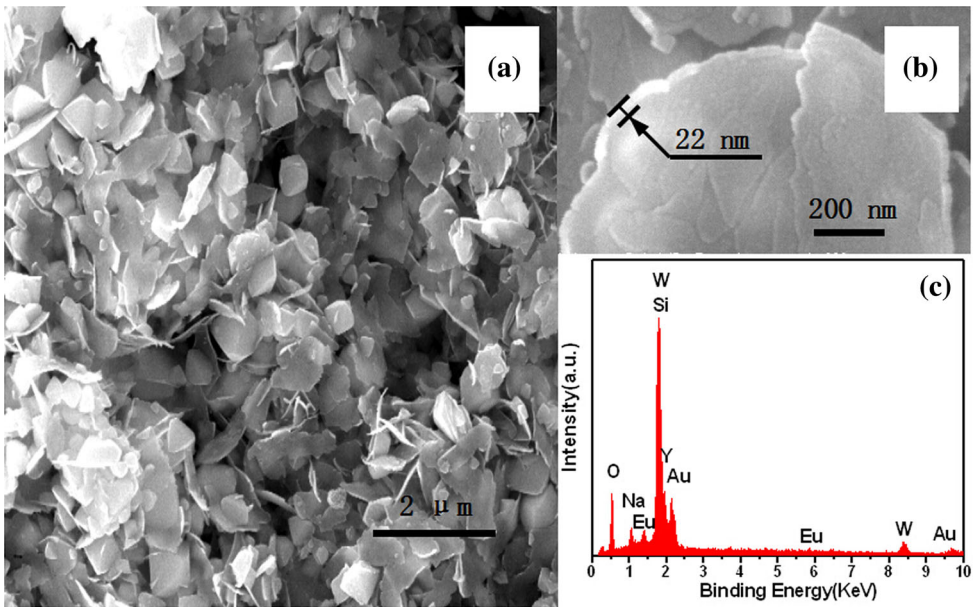

Fig. 2 FESEM images (**a**, **b**) and EDS pattern (**c**) of NaY $(WO_4)_2$:0.03Eu^{3+} phosphor

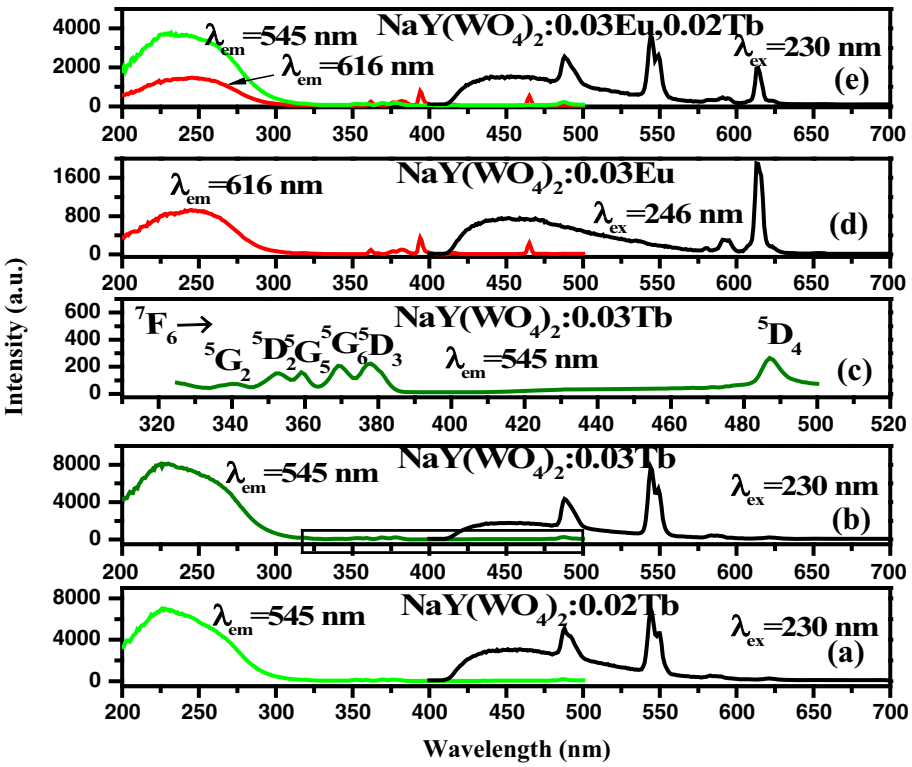

Fig. 3 PL and PLE spectra of $NaY(WO_4)_2$:0.02Tb^{3+} (**a**); $NaY(WO_4)_2$:0.03Tb^{3+} (**b**); expansion in 325–500 nm for PLE spectra of $NaY(WO_4)_2$:0.03Tb^{3+} (**c**); $NaY(WO_4)_2$:0.03Eu^{3+} (**d**); $NaY(WO_4)_2$:0.03Eu^{3+}, 0.02Tb^{3+} (**e**) phosphors

of Eu^{3+} reveals the broad band from 200 to 310 nm, which is charge transfer band (CTB) caused by the charge transfer from the completely filled $2p^6$ orbital of O^{2-} ions to the partially filled $4f^6$ orbital of the Eu^{3+} ions as well as the charge transfer between O^{2-} and W^{6+}, which indicates the energy transfer from WO_4^{2-} groups to Eu^{3+} ions [27, 37, 38]. For a clear understanding, the broad band was also deconvolved with Gaussian fitting, which has been shown in Fig. 4b. The peak located at 234 nm is due to the CTB of Eu^{3+}–O^{2-} and the peak centered at 262 nm is due to the CTB of WO_4^{2-}. There are also some sharp excitation peaks at the long wavelength in the PLE spectrum of Eu^{3+} doped $NaY(WO_4)_2$. They correspond to f-f transitions of Eu^{3+} assigned to the transitions of ($^7F_0$–$^5D_4$) at 363 nm, ($^7F_0$–$^5L_7$) at 385 nm, ($^7F_0$–$^5L_6$) at 395 nm, ($^7F_0$–$^5D_3$) at 416 nm, ($^7F_0$–$^5D_2$) at 466 nm. These excitation peaks indicate that the phosphor can strongly absorb UV, violet and blue light to obtain Eu^{3+} emission. Upon excitation with 246 nm, $NaY(WO_4)_2$:Eu^{3+} phosphor exhibits a board blue emission attributed to the transition of WO_4^{2-} in short wavelength region and some high intense emission peaks corresponding to the transitions of Eu^{3+} in long wavelength region, whose positions are at 579 nm ($^5D_0$–$^7F_0$), 591 nm ($^5D_0$–$^7F_1$), 616 nm ($^5D_0$–$^7F_2$), respectively. The strongest emission is observed due to the $^5D_0$–$^7F_2$ electric dipole transition (at 616 nm), which is about 5.64 times stronger than that of the magnetic dipole transition $^5D_0 \rightarrow {}^7F_1$ (at 591 nm), indicating that Eu^{3+} ions are positioned at the sites without inversion symmetry in the $NaY(WO_4)_2$ host [30, 39]. Furthermore, in Fig. 3d, it can be clearly seen that there is a significant spectral overlap between the broad WO_4^{2-} emission band and several excitation bands of Eu^{3+} ions located at 416 and 466 nm, indicating a favourable condition for possible energy transfer from WO_4^{2-} group to Eu^{3+} ions. This interesting phenomenon can also be observed in $NaY(WO_4)_2$:Tb^{3+} sample in both Fig. 3a, b, confirming the energy transfer between WO_4^{2-} group and Tb^{3+} ions. However, comparing the energy transfer between WO_4^{2-} and Eu^{3+} to that between WO_4^{2-} and Tb^{3+}, it is well known that the latter is much more efficient (Fig. 3b, d). This standpoint has also been reported by Liao et al. [40]. Figure 3e illustrates the PLE and PL spectra of $NaY(WO_4)_2$:0.03Eu^{3+}, 0.02Tb^{3+} phosphor. It can be noted that in the PLE spectrum, with the different monitoring wavelengths (545 nm for Tb^{3+} and 616 nm for Eu^{3+}), the broad band from 200 to 300 nm monitored by 545 nm is much stronger than that of monitored by 616 nm, further confirming that the more efficient energy transfer between WO_4^{2-} and Tb^{3+} (Fig. 3e, left). In the PL spectra of $NaY(WO_4)_2$:0.03Eu^{3+}, 0.02Tb^{3+}, it is observed both red characteristic emission and green characteristic emission and the emission intensity of Eu^{3+} is considerably enhanced compared to that of single Eu^{3+} doped sample (Fig. 3d), while the emission intensity of Tb^{3+} is distinctly decreased (Fig. 3b) because of energy transfer from Tb^{3+} to Eu^{3+}. The energy transfer between Tb^{3+} and Eu^{3+} can be confirmed by excitation spectrum of $NaY(WO_4)_2$:0.03Eu^{3+}, 0.02Tb^{3+} sample monitored at

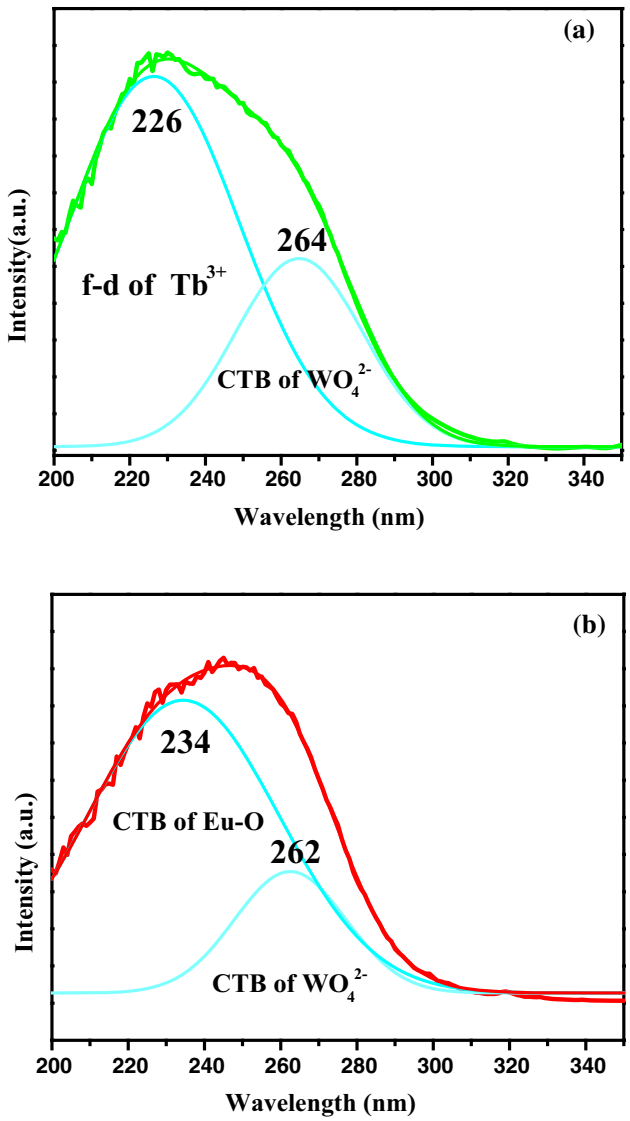

Fig. 4 Gaussian fitting curves of the broad band from 200 to 300 nm for the $NaY(WO_4)_2$:0.03Tb^{3+} (**a**) and $NaY(WO_4)_2$:0.03Eu^{3+} (**b**) phosphors

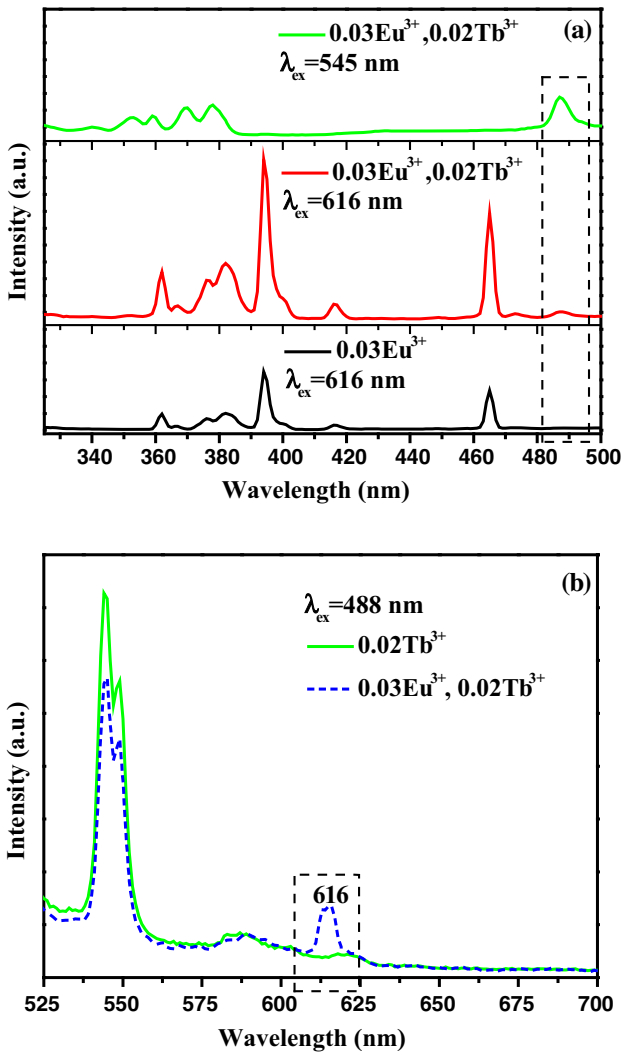

Fig. 5 PLE spectra of $NaY(WO_4)_2$:0.03Eu^{3+}, 0.02Tb^{3+} (λ_{em} = 545 and 616 nm) and $NaY(WO_4)_2$:0.03Eu^{3+} (λ_{em} = 616 nm) (**a**); PL spectra of $NaY(WO_4)_2$:0.03Eu^{3+}, 0.02Tb^{3+} (*dash line*) and $NaY(WO_4)_2$:0.02Tb^{3+} (*solid line*) (λ_{ex} = 488 nm) (**b**)

616 nm (Fig. 5). There is an excitation peak at about 488 nm (transition $^7F_6 \rightarrow {}^5D_4$ of Tb^{3+}). In emission spectrum of Tb^{3+} excited at 488 nm, there is no peak in range of 600–625 nm in $NaY(WO_4)_2$:0.02Tb^{3+} (solid line in Fig. 5b), but in $NaY(WO_4)_2$:0.03Eu^{3+}, 0.02Tb^{3+} (dash line in Fig. 5b) there is a peak of Eu^{3+} at 616 nm. Thus, emission intensity of Eu^{3+} excited at 488 nm is attributed to energy transfer from Tb^{3+} to Eu^{3+}.

In order to understand the energy transfer process, a series of samples were prepared. The Tb^{3+} mole content was fixed at 0.02 and the doping molar concentration of Eu^{3+} was varied from 0.001 to 0.03. Figure 6 depicts the variation of PL spectra and emission intensity of Tb^{3+} and Eu^{3+} in the $NaY(WO_4)_2$:xEu^{3+}, 0.02Tb^{3+} samples with varying molar concentration of Eu^{3+} under excitation at 230 nm. It is noted that the emission intensities of Tb^{3+} ($^5D_4 \rightarrow {}^7F_6$ at 488 nm, $^5D_4 \rightarrow {}^7F_5$ at 545 nm) decrease remarkably while the PL intensities of Eu^{3+} ($^5D_0 \rightarrow {}^7F_2$ at 616 nm) gradually increase with increasing Eu^{3+} molar concentration from 0.001 to 0.03, indicating the enhancement of energy transfer from the Tb^{3+} ions to Eu^{3+} ions.

To further validate the process of energy transfer, the fluorescence lifetimes τ for Tb^{3+} ($^5D_4 \rightarrow {}^7F_5$ at 545 nm) with different Eu^{3+} concentrations are measured and presented in Fig. 7. The decay behaviour of Tb^{3+} can be expressed as

$$I = I_0 + A\exp(-t/\tau) \quad (1)$$

with the Eu^{3+} concentration changing from 0.005 to 0.03 in the $NaY(WO_4)_2$:xEu^{3+}, 0.02Tb^{3+} phosphors, the integrated intensities of Tb^{3+} emissions also monotonically

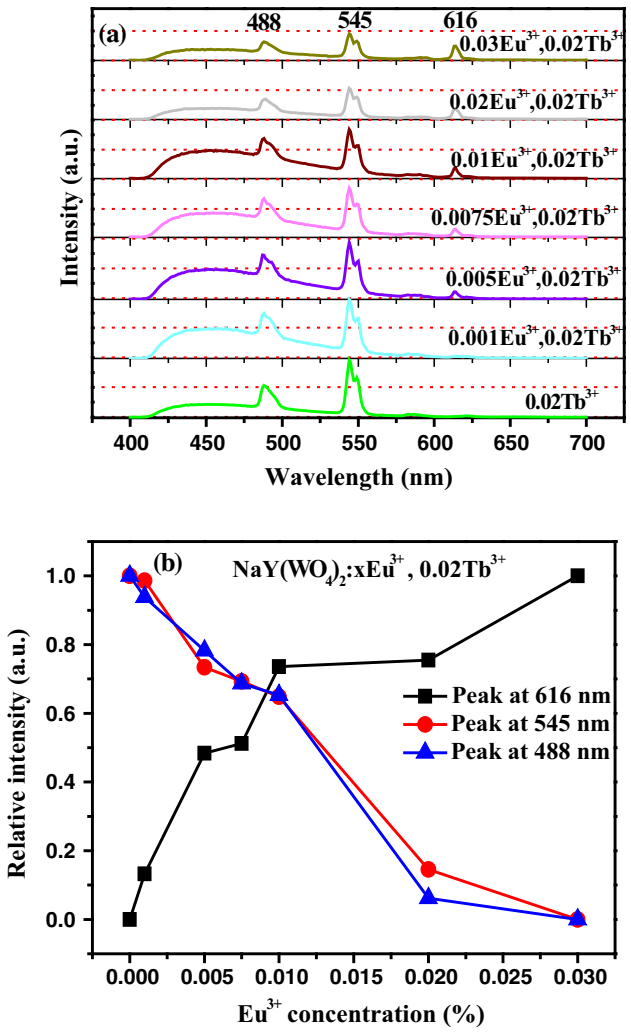

Fig. 6 Series of PL spectra of $NaY(WO_4)_2$:xEu^{3+}, $0.02Tb^{3+}$ (x = 0, 0.001, 0.005, 0.0075, 0.01, 0.02, 0.03) under UV excitation (λ_{ex} = 230 nm) (**a**); dependence of the emission intensity at different wavelength on Eu^{3+} concentration (**b**)

decrease from 0.9015 times to 0.5144 times as that of $NaY(WO_4)_2$:$0.02Tb^{3+}$. The line shown the relationship between the fluorescence lifetimes of the Tb^{3+} and Eu^{3+} doping concentration tends to be a non-exponential function with increasing Eu^{3+} concentration (Fig. 7, Inset), strongly demonstrating the characteristics of energy transfer between Tb^{3+} and Eu^{3+}. As reported, the luminescence intensities of various rare earth ions can be enhanced or quenched by the energy transfer from other co-doped rare earth ions [22]. Moreover, it is well-known that an effective energy transfer between Tb^{3+} and Eu^{3+} can take place in several hosts, such as molybdates [41], yttria [42], and tungstates [43]. The energy-transfer efficiency η_T can be calculated using the following formula [44]:

$$\eta_T = 1 - \tau/\tau_0 \quad (2)$$

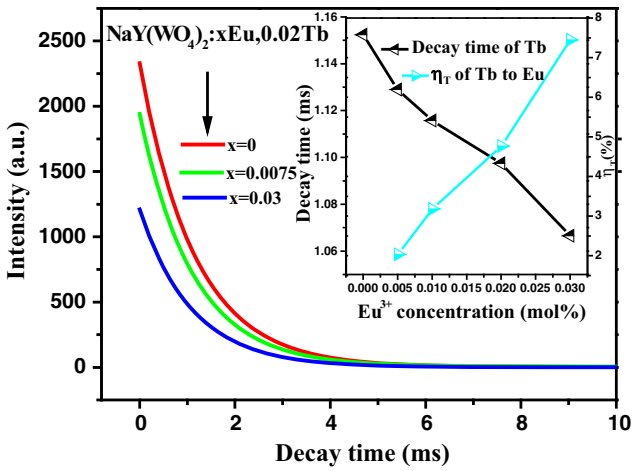

Fig. 7 Decay curves for the luminescence of Tb^{3+} ions in $NaY(WO_4)_2$:xEu^{3+},$0.02Tb^{3+}$ samples. (excited at 230 nm, monitored at 545 nm). *Inset* dependence of the fluorescence lifetime of the Tb^{3+} and energy transfer efficiency η_T on Eu^{3+} doping concentration in $NaY(WO_4)_2$:xEu^{3+}, $0.02Tb^{3+}$ phosphors

where τ and τ_0 are the lifetimes for Tb^{3+} with and without the Eu^{3+} ions. The energy-transfer efficiency is calculated as a function of Eu^{3+} concentrations and is shown in the inset of Fig. 7. It can be seen that the efficiency η_T increases with increasing Eu^{3+} concentration and reaches 7.44861 % at x = 0.03. This is because the probability of the energy transfer from Tb^{3+} to Eu^{3+} is proportional to R^{-6} (R is the average distance between Tb^{3+} and Eu^{3+}). With the increase of Eu^{3+} concentration, the average distance (R) between Tb^{3+} and Eu^{3+} is reduced, so the energy transfer efficiency is increased [22].

A schematic model proposed for the probable ways of energy transfer in Tb^{3+} and Eu^{3+} co-doped $NaY(WO_4)_2$ is shown in Fig. 8. During the excitation process, the electrons situated at oxygen 2p states absorb energies of photons from UV. As consequence of this phenomenon, the energetic electrons are promoted to tungsten 5d states located near the conductor band [45, 46]. When the electrons fall back to lower energy states again via blue emission and energy transfer to Eu^{3+} and Tb^{3+} ions, and some energy is lost by cross relaxation [47]. Furthermore, the $^5D_4$–$^7F_6$, $^5D_4$–$^7F_5$ or $^5D_4$–$^7F_4$ ($^5D_4$–$^7F_3$) emissions of Tb^{3+} overlap well with the absorption bands $^7F_0$–$^5D_2$ ($^7F_0$–$^5D_1$), $^7F_0$–$^5D_1$ or $^7F_0$–$^5D_0$ of Eu^{3+}, respectively, and thus the energy transfer also occurs between Tb^{3+} and Eu^{3+} through the cross-relaxation process. In order to obtain the multicolor light emission, it is necessary to control the energy transfer efficiency by selecting a suitable excitation wavelength for Tb^{3+} and Eu^{3+} co-doped samples. So we chose the board band area as excitation wavelength.

Generally, the energy transfer from a sensitizer to an activator in a phosphor system may take place via

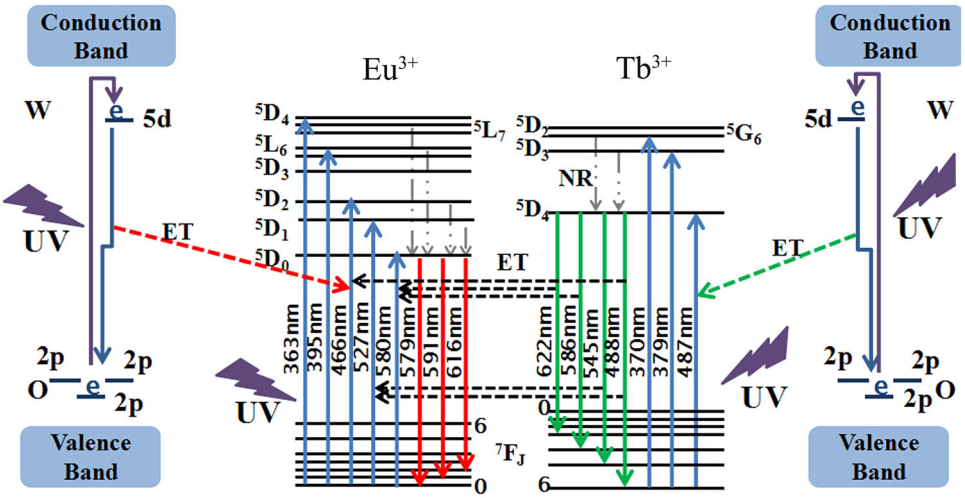

Fig. 8 Schematic energy-level diagram showing the excitation and emission mechanism of $NaY(WO_4)_2$:Eu^{3+}, Tb^{3+} phosphors (*ET* energy transfer; *NR* non radiative)

exchange interaction or multipolar interaction. Based on Dexter's energy transfer formula of multipolar interaction and Reisfeld's approximation, the following equation can be used to analyze the potential mechanism:

$$\eta_{so}/\eta_s \propto C^{n/3} \quad (3)$$

in which η_{so} and η_s is the intrinsic luminescence quantum efficiency of the Tb^{3+} ions without and with the existence of activator Eu^{3+}; and C is the doped concentration of Eu^{3+}. The values of η_{so}/η_s can be approximately calculated by the ratio of related luminescence intensities (I_{so}/I_s), where I_{so} is the intrinsic luminescence intensity of Tb^{3+}, and I_s is the luminescence intensity of Tb^{3+} in the presence of Eu^{3+}. When the value of n is 6, 8 or 10, the interaction corresponds to dipole–dipole, dipole–quadrupole, or quadrupole–quadrupole, respectively. The I_{so}/I_s plots are illustrated in Fig. 9 and the plots are used linear fitting. It can be clearly seen that when n = 6, linear fitting result is the best, implying that energy transfer from Tb^{3+} to Eu^{3+} occurs via a dipole–dipole mechanism.

We have studied the CIE values of the suite of $NaY(WO_4)_2$:xEu^{3+}, 0.02Tb^{3+} phosphors. The CIE chromaticity coordinates for the phosphors excited at 230 and 395 nm have been calculated, which are represented in the CIE diagram of Fig. 10. For the $NaY(WO_4)_2$:Eu^{3+}, Tb^{3+} phosphors, when excited at 230 nm, the trend of their color tones changes from blue to white by adjusting the doping concentration of Eu^{3+}, the corresponding chromaticity coordinates are (0.1799, 0.2716), (0.1818, 0.2590), (0.1842, 0.2558), (0.2078, 0.2910) and (0.2244, 0.2805), respectively. Furthermore, the color tone of the phosphors shifts gradually from white (which is represented at point 7) to red with exciting at 395 nm. The corresponding chromaticity coordinates are listed in Table 2. Therefore, from Fig. 10 and Table 2, it can be well seen that multiple colors are achieved by reasonable adjusting the doping

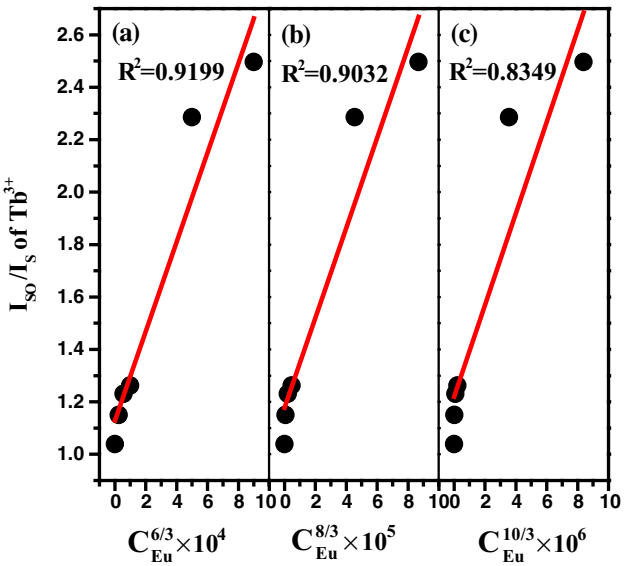

Fig. 9 Dependence of I_{so}/I_s of Tb^{3+} on **a** $C_{Eu}^{6/3} \times 10^4$, **b** $C_{Eu}^{8/3} \times 10^5$, and **c** $C_{Eu}^{10/3} \times 10^6$ in the $NaY(WO_4)_2$:xEu^{3+}, 0.02Tb^{3+} phosphors

concentration of Eu^{3+} in co-doped phosphors or through altering properly different excitation wavelengths. Moreover, the white-light emission is obtained using 395 nm as pumping source, which can find potential for WLEDs.

4 Conclusions

In summary, Eu^{3+} and/or Tb^{3+} doped $NaY(WO_4)_2$ nanoplates were prepared by one-step hydrothermal method at 260 °C for 2 h. The as-prepared Eu^{3+} or Tb^{3+} doped samples show strong red and green emission. And the energy transfer of WO_4^{2-} to Tb^{3+} is more efficient. In addition, in the case of Eu^{3+} and Tb^{3+} co-doped systems, an efficient and strong energy transfer occurs from Tb^{3+} to

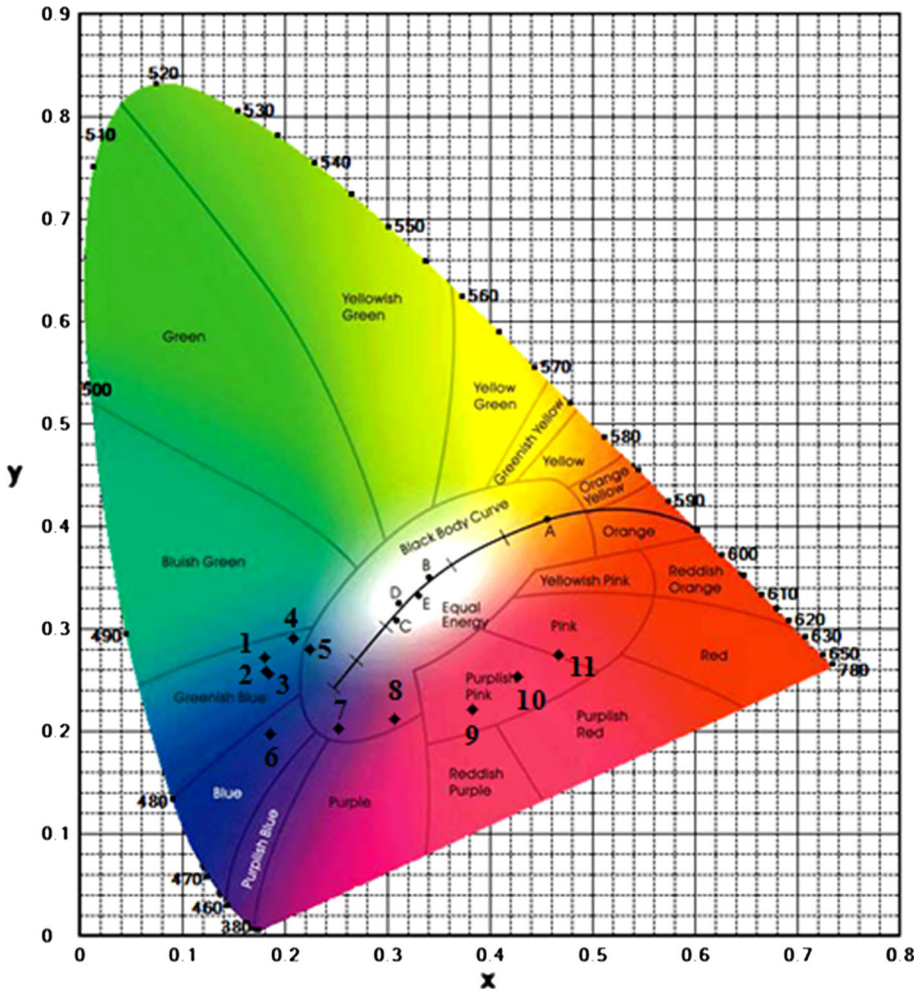

Fig. 10 CIE chromaticity diagram of the selected $NaY(WO_4)_2:Eu^{3+}$, Tb^{3+} phosphors under 230 nm (point 1–5), 246 nm (point 6) and 395 nm (point 7–11) excitations

Table 2 The corresponding chromaticity coordinates of the selected $NaY(WO_4)_2:Eu^{3+},Tb^{3+}$ phosphors

Samples	Label	Excitation wavelengths (nm)	CIE chromaticity coordinates	Colors
$NaY(WO_4)_2$:0.02Tb^{3+}	1	$\lambda_{ex} = 230$	(0.1799, 0.2716)	Greenish blue
$NaY(WO_4)_2$:0.005Eu^{3+}, 0.02Tb^{3+}	2	$\lambda_{ex} = 230$	(0.1818, 0.2590)	Greenish blue
	7	$\lambda_{ex} = 395$	(0.2519, 0.2020)	White
$NaY(WO_4)_2$:0.01Eu^{3+}, 0.02Tb^{3+}	3	$\lambda_{ex} = 230$	(0.1842, 0.2558)	Greenish blue
	8	$\lambda_{ex} = 395$	(0.3067, 0.2124)	White
$NaY(WO_4)_2$:0.02Eu^{3+}, 0.02Tb^{3+}	4	$\lambda_{ex} = 230$	(0.2078, 0.2910)	Greenish blue
	9	$\lambda_{ex} = 395$	(0.3833, 0.2220)	Purplish pink
$NaY(WO_4)_2$:0.03Eu^{3+}, 0.02Tb^{3+}	5	$\lambda_{ex} = 230$	(0.2244, 0.2805)	White
	10	$\lambda_{ex} = 395$	(0.4261, 0.2530)	Purplish pink
$NaY(WO_4)_2$:0.03Eu^{3+}	6	$\lambda_{ex} = 246$	(0.1859, 0.1969)	Blue
	11	$\lambda_{ex} = 395$	(0.4663, 0.2741)	Pink

Eu^{3+} via a dipole–dipole mechanism. And the photoluminescence emission color tones change from greenish blue to pink by different excitation wavelengths, which may make them excellent candidates in solid-state lighting. Particularly, white light emission is exhibited with 395 nm irradiation potentially finding applications in WLEDs.

Acknowledgments This work was supported by the National Natural Science Foundation of P.R. China (NSFC) (Grant Nos. 51072026, 51573023) and the Development of Science and Technology Plan Projects of Jilin Province (Grant No. 20130206002GX).

References

1. W.B. Im, Y.I. Kim, H.S. Yoo, D.Y. Jeon, Luminescent and structural properties of $(Sr_{1-x}, Ba_x)_3MgSi_2O_8:Eu^{2+}$: effects of Ba content on the $Eu2^+$ site preference for thermal stability. Inorg. Chem. **48**, 557–564 (2009)
2. Z. Wang, G. Li, Z. Quan, D. Kong, X. Liu, M. Yu, J. Lin, Nanostructured $CaWO_4$, $CaWO_4:Pb^{2+}$ and $CaWO_4:Tb^{3+}$ particles: polyol-mediated synthesis and luminescent properties. J. Nanosci. Nanotechno. **7**, 602–609 (2007)
3. G. Blasse, B.C. Grabmaier, *Luminescent Materials* (Springer, Berlin, 1994)
4. L.L. Beecroft, C.K. Ober, Nanocomposite materials for optical applications. Chem. Mater. **9**, 1302–1317 (1997)
5. T. Hashimoto, F. Wu, J.S. Speck, S. Nakamura, A GaN bulk crystal with improved structural quality grown by the ammonothermal method. Nat. Mater. **6**, 568–571 (2007)
6. R. Mueller-Mach, G. Mueller, M.R. Krames, H.A. Höppe, F. Stadler, W. Schnick, T. Juestel, P. Schmidt, Highly efficient all-nitride phosphor-converted white light emitting diode. Phys. Status Solidi A **202**, 1727–1732 (2005)
7. M. Kottaisamy, K. Horikawa, H. Kominami, T. Aoki, N. Azuma, T. Nakamura, Y. Nakanishi, Y. Hatanaka, Synthesis and characterization of fine particle $Y_2O_2S:Eu$ red phosphor at low-voltage excitation. J. Electrochem. Soc. **147**, 1612–1616 (2000)
8. K. Murakami, H. Kudo, T. Taguchi, M. Yoshimo, Compound semiconductor lighting based on InGaN ultraviolet LED and ZnS phosphor system, in *2000 IEEE International Symposium on Compound Semiconductors* (2000), pp. 449–454
9. Y. Hu, W. Zhuang, H. Ye, S. Zhang, Y. Fang, X. Huang, Preparation and luminescent properties of $(Ca_{1-x}, Sr_x)S:Eu^{2+}$ red-emitting phosphor for white LED. J. Lumin. **111**, 139–145 (2005)
10. Y. Sato, N. Takahashi, S. Sato, Full-color fluorescent display devices using a near-UV light-emitting diode. Jpn. J. Appl. Phys., Part 2 **35**, L838–L839 (1996)
11. F. Lei, B. Yan, H.H. Chen, J.T. Zhao, Surfactant-assisted hydrothermal synthesis of Eu^{3+}-doped white light hydroxyl sodium yttrium tungstate microspheres and their conversion to $NaY(WO_4)_2$. Inorg. Chem. **48**, 7576–7584 (2009)
12. Y. Zheng, H. You, K. Liu, Y. Song, G. Jia, Y. Huang, M. Yang, L. Zhang, G. Ning, Facile selective synthesis and luminescence behavior of hierarchical $NaY(WO_4)_2:Eu^{3+}$ and $Y_6WO_{12}:Eu^{3+}$. CrystEngComm **13**, 3001–3007 (2011)
13. J. Liu, J.M. Cano-Torres, C. Cascales, F. Esteban-Betegón, M.D. Serrano, V. Volkov, C. Zaldo, M. Rico, U. Griebner, V. Petrov, Growth and continuous-wave laser operation of disordered crystals of $Yb^{3+}:NaLa(WO_4)_2$ and $Yb^{3+}:NaLa(MoO_4)_2$. Phys. Status Solidi A **202**, R29–R31 (2005)
14. A. Garcia-Cortes, C. Cascales, A. de Andres, C. Zaldo, E.V. Zharikov, K.A. Subbotin, S. Bjurshagen, V. Pasiskevicius, M. Rico, Raman scattering and Nd^{3+} laser operationin $NaLa(WO_4)_2$. IEEE J. Quantum Electron. **43**, 157–167 (2007)
15. S. Huang, X. Zhang, L. Wang, L. Bai, J. Xu, C. Li, P. Yang, Controllable synthesis and tunable luminescence properties of $Y_2(WO_4)_3:Ln^{3+}$ (Ln = Eu, Yb/Er, Yb/Tm and Yb/Ho) 3D hierarchical architectures. Dalton Trans. **41**, 5634–5642 (2012)
16. X. Liu, W. Xiang, F. Chen, Z. Hu, W. Zhang, Synthesis and photoluminescence characteristics of Dy^{3+} doped $NaY(WO_4)_2$ phosphor. Mater. Res. Bull. **48**, 281–285 (2013)
17. Y.S. Zhao, H. Fu, F. Hu, A.D. Peng, J. Yao, Multicolor emission from ordered assemblies of organic 1D nanomaterials. Adv. Mater. **19**, 3554–3558 (2007)
18. A.A. Kaminskii, H.J. Eichler, K.-I. Ueda, N.V. Klassen, B.S. Redkin, L.E. Li, J. Findeisen, D. Jaque, J. García-Sole, J. Fernández, R. Balda, Properties of Nd^{3+}-doped and undoped tetragonal $PbWO_4$, $NaY(WO_4)_2$, $CaWO_4$, and undoped monoclinic $ZnWO_4$ and $CdWO_4$ as laser-active and stimulated raman scattering-active crystals. Appl. Opt. **38**, 4533–4547 (1999)
19. Y.R. Do, Y.D. Huh, Optical properties of potassium Europium tungstate phosphors. J. Electrochem. Soc. **147**, 4385–4388 (2000)
20. S. Neeraj, N. Kijima, A.K. Cheetham, Novel red phosphors for solid-state lighting: the system $NaM(WO_4)_{2-x}(MoO_4)_x:Eu^{3+}$ (M = Gd, Y, Bi). Chem. Phys. Lett. **387**, 2–6 (2004)
21. E. Pavitra, G.S.R. Raju, Y.H. Ko, J.S. Yu, A novel strategy for controllable emissions from Eu^{3+} or Sm^{3+} ions co-doped $SrY_2O_4:Tb^{3+}$ phosphors. Phys. Chem. Chem. Phys. **14**, 11296–11307 (2012)
22. M. Shang, G. Li, X. Kang, D. Yang, D. Geng, J. Lin, Tunable Luminescence and Energy Transfer properties of $Sr_3AlO_4F:RE^{3+}$ (RE = Tm/Tb, Eu, Ce) Phosphors. ACS Appl. Mater. Interfaces **3**, 2738–2746 (2011)
23. Y. Tian, B. Chen, B. Tian, N. Yu, J. Sun, X. Li, J. Zhang, L. Cheng, H. Zhong, Q. Meng, R. Hua, Hydrothermal synthesis and tunable luminescence of persimmon-like sodium lanthanum tungstate:Tb^{3+}, Eu^{3+} hierarchical microarchitectures. J. Colloid Interface Sci. **393**, 44–52 (2013)
24. C. Zhang, H. Liang, S. Zhang, C. Liu, D. Hou, L. Zhou, G. Zhang, J. Shi, Efficient sensitization of Eu^{3+} emission by Tb^{3+} in $Ba_3La(PO_4)_3$ under VUV-UV excitation: energy transfer and tunable emission. J. Phys. Chem. C **116**, 15932–15937 (2012)
25. Z. Hou, Z. Cheng, G. Li, W. Wang, C. Peng, C. Li, P.A. Ma, D. Yang, X. Kang, J. Lin, Electrospinning-derived $Tb_2(WO_4)_3:Eu^{3+}$ nanowires: energy transfer and tunable luminescence properties. Nanoscale **3**, 1568–1574 (2011)
26. L. Li, L. Liu, W. Zi, H. Yu, S. Gan, G. Ji, H. Zou, X. Xu, Synthesis and luminescent properties of high brightness $MLa(WO_4)_2:Eu^{3+}$ (M = Li, Na, K) and $NaRE(WO_4)_2:Eu^{3+}$ (RE = Gd, Y, Lu) red phosphors. J. Lumin. **143**, 14–20 (2013)
27. X. Liu, W. Xiang, F. Chen, W. Zhang, Z. Hu, Synthesis and photoluminescence of Tb^{3+} activated $NaY(WO_4)_2$ phosphors. Mater. Res. Bull. **47**, 3417–3421 (2012)
28. S. Huang, D. Wang, Y. Wang, L. Wang, X. Zhang, P. Yang, Self-assembled three-dimensional $NaY(WO_4)_2:Ln^{3+}$ architectures: hydrothermal synthesis, growth mechanism and luminescence properties. J. Alloys Compd. **529**, 140–147 (2012)
29. N. Xue, X. Fan, Z. Wang, M. Wang, Mater. Lett. **61**, 1576 (2007)
30. F. Wang, X. Fan, D. Pi, Z. Wang, M. Wang, Hydrothermal synthesis and luminescence behavior of rare-earth-doped $NaLa(WO_4)_2$ powders. J. Solid State Chem. **178**, 825–830 (2005)
31. S. Perets, R.Z. Shneck, R. Gajic, A. Golubovic, Z. Burshtein, Vibrational spectra of sodium gadolinium tungstate $NaGd(WO_4)_2$ single crystals: observation of spatial dispersion. Vib. Spectrosc. **49**, 110–117 (2009)
32. X. Qian, X. Pu, D. Zhang, L. Li, M. Li, S. Wu, Combustion synthesis and luminescence properties of $NaY_{1-x}Eu_x(WO_4)_2$ phosphors. J. Lumin. **131**, 1692–1695 (2011)
33. Y. Liu, Y.X. Liu, G.X. Liu, X.T. Dong, J.X. Wang, Up/Down conversion, tunable photoluminescence and energy transfer properties of $NaLa(WO_4)2:Er^{3+}$, Eu^{3+} phosphors. RSC Adv. **5**, 97995–98003 (2015)
34. Y. Liu, Y.X. Liu, G.X. Liu, X.T. Dong, J.X. Wang, W.S. Yu, Luminescence, energy transfer and tunable color properties of a single-component Tb^{3+} or/and Sm^{3+} doped $NaGd(WO_4)_2$ phosphors with UV excitation for WLEDs. RSC Adv. **4**, 58708–58716 (2014)

35. Y. Liu, Y.X. Liu, G.X. Liu, J.X. Wang, X.T. Dong, W.S. Yu, A single component and warm-white-emitting phosphor $NaGd(WO_4)_2$:Tm^{3+}, Dy^{3+}, Eu^{3+}: synthesis, luminescence, energy transfer and tunable color. Inorg. Chem. **53**, 11457–11466 (2014)
36. Y.Y. Jiang, Y. Liu, G.X. Liu, X.T. Dong, J.X. Wang, W.S. Yu, Q. Dong, Surfactant-assisted hydrothermal synthesis of octahedral structured $NaGd(MoO_4)_2$:Eu^{3+}/Tb^{3+} and tunable photoluminescent properties. Opt. Mater. **36**, 1865–1870 (2014)
37. P. Jia, X. Liu, Y. Luo, M. Yu, J. Lin, Sol–Gel synthesis and characterization of SiO_2@NaGd $(WO_4)_2$:Eu^{3+} core-shell-structured spherical phosphor. J. Electrochem. Soc. **154**, J39–J43 (2007)
38. C.H. Chiu, M.F. Wang, C.S. Lee, T.M. Chen, Structural, spectroscopic and photoluminescence studies of $LiEu(WO_4)_{2-x}(MoO_4)_x$ as a near-UV convertible phosphor. J. Solid State Chem. **180**, 619–627 (2007)
39. N. Xue, X. Fan, Z. Wang, M. Wang, Synthesis process and the luminescence properties of rare earth doped $NaLa(WO_4)_2$ nanoparticles. J. Phys. Chem. Solids **69**, 1891–1896 (2008)
40. J. Liao, S. Zhang, H. You, H.-R. Wen, J.L. Chen, W. You, Energy transfer and luminescence properties of Eu^{3+}-doped $NaTb(WO_4)_2$ phosphor prepared by a facile hydrothermal method. Opt. Mater. **33**, 953–957 (2011)
41. A. Khanna, P.S. Dutta, Narrow spectral emission $CaMoO_4$:Eu^{3+}, Dy^{3+}, Tb^{3+} phosphor crystals for white light emitting diodes. J. Solid State Chem. **198**, 93–100 (2013)
42. D. Tu, Y. Liang, R. Liu, D. Li, Eu/Tb ions co-doped white light luminescence Y_2O_3 phosphors. J. Lumin. **131**, 2569–2573 (2011)
43. M.V. Nazarov, D.Y. Jeon, J.H. Kang, E.J. Popovici, L.E. Muresan, M.V. Zamoryanskaya, B.S. Tsukerblat, Luminescence properties of europium–terbium double activated calcium tungstate phosphor. Solid State Commun. **131**, 307–311 (2004)
44. P.I. Paulose, G. Jose, V. Thomas, N.V. Unnikrishnan, M.K.R. Warrier, Sensitized fluorescence of Ce^{3+}/Mn^{2+} system in phosphate glass. J. Phys. Chem. Solids **64**, 841–846 (2003)
45. J.C. Sczancoski, L.S. Cavalcante, N.L. Marana, R.O. da Silva, R.L. Tranquilin, M.R. Joya, P.S. Pizani, J.A. Varela, J.R. Sambrano, M.S. Li, E. Longo, J. Andrés, Electronic structure and optical properties of $BaMoO_4$ powders. Curr. Appl. Phys. **10**, 614–624 (2010)
46. V.M. Longo, L.S. Cavalcante, R. Erlo, V.R. Mastelaro, A.T. de Figueiredo, J.R. Sambrano, S. de Lázaro, A.Z. Freitas, L. Gomes, N.D. Vieira Jr., J.A. Varela, E. Longo, Strong violet-blue light photoluminescence emission at room temperature in $SrZrO_3$: joint experimental and theoretical study. Acta Mater. **56**, 2191–2202 (2008)
47. A.M. Li, D.K. Xu, H. Lin, S.H. Yang, Y.Z. Shao, Y.L. Zhang, Z.Q. Chen, Facile morphology-controllable hydrothermal synthesis and color tunable luminescence properties of $NaGd(MoO_4)_2$:Eu^{3+}, Tb^{3+} microcrystals. RSC Adv. **5**, 45693–45702 (2015)